Indonesian Journal of Science & Technology

Journal homepage: http://ejournal.upi.edu/index.php/ijost/

Risk-Based Leak Analysis of an LPG Storage Tank: A Case Study

Suroto Munahar[1], Bagiyo Condro Purnomo[1], Nanda Ferdiansyah[2], Eko Muh Widodo[2], Moehamad Aman[2], Retno Rusdjijati[2], Muji Setiyo[1]*

[1] Department of Automotive Engineering, Universitas Muhammadiyah Magelang, Indonesia
[2] Department of Industrial Engineering, Universitas Muhamadiyah Magelang, Indonesia
Correspondence: E-mail: muji@unimma.ac.id

ABSTRACT

Liquified petroleum gas (LPG) storage tanks are essential components for storing and distributing fuels. However, system failures due to inspection flaws increase the risk of leaks, fires, and explosions. Therefore, this study discussed the development of a safety system application applied to LPG storage tanks based on a risk-based leak (RBL) analysis. Data associated with risk factor values were obtained from an LPG storage tank in a gas distributor company. The risk of failure was calculated by analyzing the probability of failure (PoF) and the consequence of failure (CoF). The results showed that the level of risk observed was medium-high with a *PoF* in category 1 at a total damage factor value of 1. Furthermore, the *CoF* in category E was positioned with a consequence analysis value of 2381.29 m^2 with an LPG storage tank life span of 33.5 years and an external inspection interval of five years.

ARTICLE INFO

Article History:
Submitted/Received 10 Sep 2021
First revised 23 Oct 2021
Accepted 06 Jan 2022
First available online 07 Jan 2022
Publication date 01 Apr 2022

Keyword:
Consequence of failure,
LPG storage tank,
Probability of failure,
Risk-based leak.

1. INTRODUCTION

Owing to its properties, liquified petroleum gas (LPG) is a popular domestic energy source used in industries, households, and transportation. Many reports are available on LPG implementation for the automotive sector (Munahar *et al*., 2021; Purnomo & Widodo, 2019; Setiyo et al., 2019), and they are still promising in the medium term (Widodo *et al*., 2019). Demand for LPG shows an increase during 2000-2020 because it is cleaner than other oil-based fuels such as diesel and gasoline (Kivevele *et al*., 2020). Clean energy is inevitable, making it interesting for researchers, scientists, and engineers to create other types of energy sources (Kareem et al., 2022; Irawan et al., 2021; Putri et al., 2021; Sihombing et al., 2021; Fauziah et al., 2021; Hidayah et al., 2021; Irawan et al., 2021).

LPG storage and distribution along the supply chain requires tanks, which carry a risk of a leak. Cracked and corroded tanks lead to leaks, fires, and even explosions. According to previous studies related to LPG distribution, 242 cases of fire outbreaks and accidents have been recorded during 1960-2003, and 74% of these incidents were due to fuel storage tank failures (Chang & Lin, 2006).

A massive fire outbreak recently occurred in Jurong, Singapore, due to a leak in the pipeline, as shown in **Figure 1a**, which caused a loss of millions of dollars (CNA, 2019). Another incident occurred in Ghana, where an LPG-carrying vehicle caught fire due to a leak, and the impact is shown in **Figure 1b** (Hazardex, 2017). A monitoring system for LPG-carrying vehicles has been developed to reduce the risk of accidents, but accidents due to leaks are still an issue that needs to be discussed (Susanto *et al*., 2019). Likewise, there was an explosion in an LPG storage tank in Chiba, Japan. This company lost 17 ships, conveying an estimated volume of 6800–85000 m^3 of LPG. The explosion generated enormous fireballs of approximately 500 m in diameter (Li *et al*., 2015).

LPG fires stemming from leaking cracks in devices tend to cause large fireballs. Bariha experimented on LPG leaks over a time period of approximately 20 min (Bariha *et al*., 2016). It was discovered that these leaks create a vast vapor cloud and, when ignited, lead to uncontrollable fireballs. The impact of the damage involves the burning of other facilities owing to radiation effects (Yi *et al*., 2019). Apart from the failure caused by cracking and corrosion, LPG leak also occurs due to overpressure caused by the evolution of shock waves and dynamic stresses accompanied by high temperatures. A storage tank with a pressure of over 200 kPa maintained in an area in which shock waves are generated is potentially dangerous (Zhang *et al*., 2020). Moreover, explosions caused by dynamic pressure at high temperatures can destroy walls that are 370 mm thick (Zhang *et al*., 2020). Regarding the distribution aspect, drivers or individuals responsible for the LPG transport tankers or vehicles need to pay attention to safety factors, especially when leaks occur in an enclosed area (Li, 2019; Zhang *et al*., 2020). It shows that when an LPG vehicle explodes in a tunnel, its effects extend for a considerable distance.

Therefore, because of the losses associated with LPG storage failures, it is necessary to adopt an adequate safety system. Currently, a risk-based inspection (RBI) analysis is being developed to prevent fire outbreaks due to oil and gas leaks. Research on the application of RBIs has been widely applied in various fields, including the development of intelligent control systems (Gallab *et al*., 2019; Singh & Pokhrel, 2018). This study applies fuzzy logic to the control of general oil and gas treatments and analyses the consequences of hazards and possible risks. As a result, an analytical approach model was designed to determine maintenance measures, although this system has not been implemented in a real-time condition.

DOI: https://doi.org/10.17509/ijost.v7i1
p- ISSN 2528-1410 e- ISSN 2527-8045

Figure 1. Effects of fire due to leak of LPG storage tanks in Singapore (a) and Ghana (b).

RBI has also been applied to welding leaks in oil pipelines (Mzad & Khelif, 2017). The proposed research is based on mechanical modeling, which illustrates the failure of weld cracks. Another study applied RBI to investigate the corrosion rate of condensate pipes (Perumal, 2014). However, the results were inaccurate because qualitative analysis methods were applied. Subsequent research has been carried out on the dangers to pipelines due to material fatigue in offshore oil refineries (Lassen, 2013). The impact of ocean waves causes uncertainty in the maintenance schedule. RBI is a preventive measure applied as a risk-based assessment of material fatigue caused by wave impact. Lassen's study conducted a risk analysis of material fatigue in offshore oil mining owing to the impact of ocean waves.

Machine learning models generated through the screening method were carried out using the RBI approach. The observed variables included measurements obtained from the oil and gas production processes (Rachman & Ratnayake, 2019). This study was designed as a model and did not adopt real-time actions.

Machine learning was developed using intelligent control system applications. Subsequently, RBI was used for the management of polyethylene material maintenance (Wang *et al*., 2011). This model can be used with equipment that works at high pressure, thereby reducing the risk of accidents and failures.

API standards are used to analyze risk in storage tanks (API, 2006; Nugroho *et al*., 2016). These standards also serve as a reference in assessing risks, designing measurable inspections, and determining maintenance schedules (Tan, Zhao yang , Li, Jianfeng , Wu, Zong zhia, Zheng, Jianhu, He, 2011). This study evaluated industrial equipment for the risk level category based on an RBI analysis. An analytical hierarchical process application (AHP) was used for the selection of maintenance strategies. However, this study did not evaluate industrial equipment based on an online system; therefore, the evaluation cannot be done in a real-time condition. According to various previous studies, the application of RBI to risk management exists in the oil and gas maintenance sector. However, only a few studies have investigated the API sector that specifically manages safety system risks in online systems based on LPG storage tanks. Therefore, this study proposes the development of such a system. The uniqueness of this research is the development of an online maintenance system so that the calculation analysis works in a real-time condition. Management can immediately know the maintenance results, which do not depend on time or place. This study used the API 581 and API 510 standards to assist in the accuracy of the risk analyses

DOI: https://doi.org/10.17509/ijost.v7i1
p- ISSN 2528-1410 e- ISSN 2527-8045

for LPG storage tanks. The RBI risk analysis level is included in the Level 1 rating; therefore, the focus is on analyzing the LPG vapor phase leak, flammability, and explosion consequences. The toxic consequences, non-flammable release consequences, non-toxic consequences, and financial consequences were analyzed in a subsequent study.

2. METHODS

The data collection scheme is illustrated in **Figure 2**. The layout of the LPG storage tank inspection was divided into six spot shells and two heads, which were each further divided into ten measurement points. Each of the spot shells and heads was examined at three points between the angles of 90, 180, and 270°. The head section was divided into two parts, namely heads A and B. The inspection method for measuring the LPG storage tank's condition used the usually effective category, which has a confidence level of 60 to 80% and nominally 20% ultrasonic manual scanning coverage. Several nomenclatures and symbols used in this study are presented in **Tables 1** and **2.**

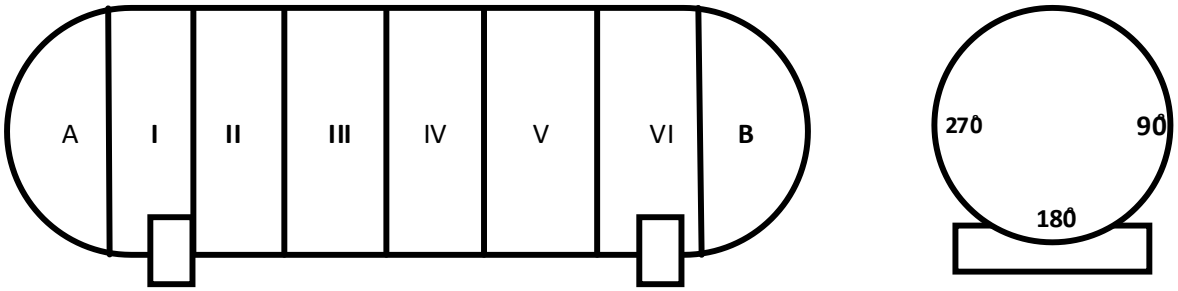

Figure 2. Set up inspection for LPG storage tank.

Table 1. Symbols used in this study.

Nomenclature	Definition
A_{rt}	Parameter damage factor
A_{rt}	Damage factor parameter
C_2	Conversion factor
C_3	Customary conversion factors of 4535.92 kg
C_d	Discharge hole coefficient
$D_f(t)$	Damage factor
D^{thin}	Damage factor of thinning
$D^{thin}\ fb$	Base damage factor for thinning
F_{AM}	Adjustment for tank maintenance per API 653 (only atmospheric storage tank)
F_{DL}	Adjustment for dead legs
F_{IP}	Adjustment for injection/mix points
F_{OM}	Adjustment to damage factor for online monitoring
F_{SM}	Adjustment for settlement (only to atmospheric storage tank bottoms)
F_{WD}	Adjustment for welded (only to atmospheric storage tanks)
$fact_{di}$	Release magnitude reduction factor
$fact_n^{IC}$	Continuous blending factor
A, B, C, D	Ideal gas constant
E	Joint efficiency
K	Factor value with a magnitude of 1
S	Allowable stress
V	Volume of the tank
k	Ideal gas specific heat ratio

DOI: https://doi.org/10.17509/ijost.v7i1
p- ISSN 2528-1410 e- ISSN 2527-8045

Table 2. Nomenclatures used in this study.

Nomenclature	Definition
age	In-service time (y)
A_n	Area of each leak hole (m^2)
CA	Area consequences (m^2)
C_p	Specific heat of release fluid (J/kmol·K)
CoF	Consequence of failure (m^2)
$C_{r,bm}$	Base metal corrosion rate (mm/y)
$C_{r,bm(short)}$	Short-term corrosions (mm/y)
$C_{r,bm(long)}$	Long-term corrosions (mm/y)
d_n	Hole diameter (mm)
G_c	Constant gravity (m/s^2)
gff	Failure frequency (failure/y)
ID	Tank's head diameter (mm)
$mass_{add,n}$	Calculation of mass of fluid added (kg)
$mass_{comp}$	Fluid analysis for each component in the inventory group (kg)
$Mass_n$	Mass leaks (kg)
P	LPG working pressure in the tank (MPa)
P_{atm}	Inner atmospheric pressure (MPa)
PoF	Probability of failure (failure/y)
P_s	Equipment pressure (MPa)
P_{trans}	Transition back pressure (MPa)
$Rate_n$	Rate calculation (kg/s)
R_i	Tank's shell radius (mm)
T	Temperature (K)
T_{act}	Recent tank wall thickness (mm)
T_{min}	Minimum wall thickness (mm)
$T_{minhead}$	Shell head wall thickness (mm)
$T_{minshell}$	Shell spot wall thickness (mm)
t_n	Release time (s)
T_{nom}	Tank wall thickness at the time of production (mm)
T_{prev}	Final thickness of the tank (mm)
T_{rd}	Tank wall thickness (mm)
W_{max8}	Flow rate for diameter 8 in (203.2 mm) (kg/s)
W_n	Leak rate calculation (kg/s)
ρ	Density of the chosen representative fluid (kg/m^3)

2.1. Risk-Based Leak (RBL)

RBL is a tank safety system analysis method derived from the RBI technique. It functions according to API Standard 581. Currently, RBI is a significant method for improving safety in the industry (Abubakirov *et al*., 2020; Song *et al*., 2021; Zwetsloot *et al*., 2020). RBL is a risk-based analysis instrument that refers to the integration of the probability of failure (*PoF*) and consequence of failure (*CoF*). According to API 581, the risk is calculated using Equation [1] (Shishesaz *et al*., 2013; Song *et al*., 2021).

$$Risk = PoF \cdot CoF \quad (1)$$

2.2. Probability of Failure (*PoF*)

This technique is used to calculate the *PoF* ($P_f(t)$) determined by the general failure frequency (gff), damage factor ($D_f(t)$), and management system factor (F_{MS}). The *PoF* is calculated using Equation [2] (Bhatia *et al*., 2019).

DOI: https://doi.org/10.17509/ijost.v7i1
p- ISSN 2528-1410 e- ISSN 2527-8045

$$P_f(t) = gff \cdot D_f(t) \cdot F_{MS} \quad (2)$$

2.2.1. The general failure frequency value

General failure frequency is an analytical instrument for tools that function according to certain specifications based on industries or lean literature sources. This also represents the deteriorating performance of the equipment. The general failure frequency values for LPG storage tanks according to the API 581 standard are included in the pressure vessel category.

2.2.2. Damage factor

RBL is supported by the damage factor $(D_f(t))$ to provide screening instruments that prioritize and optimize inspections. According to the API, the analysis of damage factors in a system has several estimates, including thinning ($D_f{}^{thin}$), component lining ($D_f{}^{elin}$), external damage ($D_f{}^{extd}$), stress corrosion cracking ($D_f{}^{scc}$), high-temperature hydrogen attack ($D_f{}^{dtha}$), mechanical fatigue ($D_f{}^{mfa}$), and brittle fracture ($D_f{}^{brit}$). However, not all estimates are used during the calculation, and the condition depends on the system requirements to be analyzed. This study only requires a thinning damage factor estimation ($D_f{}^{thin}$) with the assumption that the risk of a leak is represented by the thickness of the pressure vessel plate because the tank studied was a static tank.

2.2.3. Thinning damage factor

The procedure for analyzing thinning damage factors has nine stages, including determining the number of inspections and its effectiveness category, in-service time (age), base metal corrosion rate ($C_{r,bm}$), minimum wall thickness (T_{min}), parameter damage factor (A_{rt}), base damage factor for thinning (D^{thin} *fb*), thinning damage factors, management system factors, and calculating the time or age since the last inspection.

The determination of the inspection number and its effectiveness category is in accordance with the RBI API standard guidelines. In this study, they were both included in inspection category B. External ultrasound was used for the data collection process at the usually effective rank. Time in service (age) was calculated using Equation [3].

The corrosion rate base metal ($C_{r,bm}$) is distinguished from short-term and long-term corrosion and is calculated using Equations (4) and (5), respectively. T_{prev} is the final thickness of the tank wall, while T_{act} is the recent tank wall thickness (API, 2006). The tank wall thickness at the time of production is denoted as T_{nom}.

The shell spot wall thickness ($T_{minshell}$) and head ($T_{minhead}$) are determined by referring to Equations [6] and [7] (API, 2008), wherein, the formulas in this standard are used for the calculations in this article. The LPG working pressure in the tank is denoted by P, which also serves as its diameter. S stands for allowable stress, while E is the joint efficiency, which has a value of 1. R_i is the radius of the tank shell section, ID is the diameter of the tank head, and K is a factor with a magnitude of 1.

The damage factor parameter (A_{rt}) is calculated using Equation [8], where t_{rd} is the tank wall thickness, and CA is the corrosion allowance. The base damage factor for thinning ($D^{thin}fb$) was determined by the inspection effectiveness category. The number of inspections performed was analyzed based on the thinning damage factor, as shown in **Table 3**.

The damage factor of thinning (D^{thin}) was determined based on Equation (9), which includes injection or mix points (F_{IP}), dead legs (F_{DL}), welded construction (F_{WD}), tank maintenance per API 653 (F_{AM}), settlement (F_{SM}), and online monitoring (F_{OM}). The calculations are shown in Equations [3]-[9].

DOI: http://doi.org/10.17509/ijost.v7i1.42916
p- ISSN 2528-1410 e- ISSN 2527-8045

Table 3. Thinning damage factors.

A_{rt}	Inspection's effectiveness								
	E	5 Inspection				6 Inspection			
		D	C	B	A	D	C	B	A
0.02	1	1	1	1	1	1	1	1	1
0.04	1	1	1	1	1	1	1	1	1
0.06	1	1	1	1	1	1	1	1	1
0.08	1	1	1	1	1	1	1	1	1
0.10	2	1	1	1	1	1	1	1	1

$$age = current\ inspection - last\ inspection \quad (3)$$

$$C_{r,bm\ (short)} = \frac{(T_{prev} - T_{act})}{age} \quad (4)$$

$$C_{r,bm(long)} = \frac{(T_{nom} - T_{act})}{(year\ betwen\ T_{nom}\ and\ T_{act})} \quad (5)$$

$$T_{minshell} = \frac{P \cdot R_i}{S \cdot E - 0.6\,P} \quad (6)$$

$$T_{minhead} = \frac{P \cdot ID \cdot K}{(2S \cdot E - 0.2P)} \quad (7)$$

$$A_{rt} = max\left(1 - \frac{t_{rd} - C_{r,bm} \cdot age}{t_{min} + CA}\right) \quad (8)$$

$$D_f^{thin} = \frac{D_{fB}^{thin} \cdot F_{IP} \cdot F_{DL} \cdot F_{WD} \cdot F_{AM} \cdot F_{SM}}{F_{OM}} \quad (9)$$

D_{fB}^{thin} is the base value of the thinning damage factor. Note that F_{OM} should not be applied if D_{fB}^{thin} is 1. F_{IP} is an injection add-on factor defined as the point at which a chemical compound (including water) is added to the mainstream. However, assuming that the equipment circuit has an injection point, the value-added factor F_{IP} is 3, and assuming that the effectiveness inspection is high owing to corrosion at the injection point, this factor is excluded. This study did not include a pipe network; therefore, the F_{IP} value is 1. F_{DL} is the pipe equipment used during the intermittent service. Assuming the equipment is in this section, the F_{DL} value is 3. However, the effectiveness of the inspection was used to determine that the corrosion potential of F_{DL} is 1. F_{WD}, F_{AM}, F_{SM} are used to denote an additional factor that only applies to atmospheric storage tanks. Subsequently, assuming that the equipment being measured is not an atmospheric storage tank, the value is 1. In addition, F_{OM} is an additional factor, and when inspected in accordance with an offline monitoring method, the value is 1.

Management system factors greatly affect the frequency of component failures, and the RBL analysis considers this fact. The evaluation of management system factors is described using API 581 in Annex 2.A and has a maximum score of 1000. The management system factor is obtained from Equation [10].

$$pscore = \frac{Score}{1000} \cdot 100\ [\ unit\ is\ \%] \quad (10)$$

Equation [11] presents an assessment of the maintenance management of LPG storage tanks. This equation was obtained from the score variable assessment. The score is an assessment variable obtained from the direct observation of LPG storage tank management. The score has a range of 0–1000. Therefore, the value of $pscore$ is entered into Equation (11) to obtain the value of F_{MS}.

$$F_{MS} = 10^{(-0.02 \cdot pscore + 1)} \quad (11)$$

2.3. The Consequence of Failure (CoF)

A consequence analysis in the RBI API assessment is carried out to help rank tools based on their risk tendencies or possibilities. This measure is used to prioritize inspections. There are two methods involved in consequence analysis: Levels 1 and 2. The Level 1 consequence analysis is simpler than the Level 2 analysis.

DOI: http://doi.org/10.17509/ijost.v7i1.42916
p- ISSN 2528-1410 e- ISSN 2527-8045

The calculation of the *CoF* involves several steps, including determining the representative fluid and its properties, size of the leak hole, leak rate, mass of available fluid in a gas leak, type of leak, impact of the detection and isolation system, rate, and mass of the leak for consequential analysis, consequences of fire and explosions, and component damage and personnel injury.

2.3.1. Determine the representative fluid

This is determined through several steps, namely fluid selection and the determination of the fluid phase and nature of the stored fluid. The representative fluid was selected based on the material contained in the equipment. According to the API 581 standard, the fluids used in this study are classified as class fluids $C_3 - C_4$ and fluid-type TYPE 0. The fluid phase characteristics of C3-C4 are shown in **Table 4**.

Moreover, before determining the *CoF* value, the ideal gas specific heat ratio (k), which is obtained from the constant pressure specific heat (C_p), must be obtained. The value for (k) is obtained from Equation [12]. In contrast, Equation [13] is used to find (C_p). The ideal gas values for A, B, C, D are properties of the representative fluids used for the Level 1 analysis. T is the temperature in Kelvin and R is the gas constant.

$$k = \frac{C_p}{C_p - R} \quad (12)$$

$$C_p = A + BT + CT^2 + DT^3 \quad (13)$$

2.3.2. Selection of leak hole size (release hole size)

The leak hole size has a maximum diameter of 406.4 mm and is used to indicate the maximum practical value for calculating the leaks. In general, equipment failures do not involve disintegration. The leak hole size is calculated by selecting the diameter (d_n), as shown in **Table 4**.

2.3.3. Leak rate calculation (W_n)

The leak rate is determined based on the physical properties of the material, its initial phase, operating process conditions, and leak hole size. It is calculated in accordance with several procedures, including selecting the leak rate equation based on the stored fluid phase. The leak rate is also calculated based on the value of P_{trans}, as stated in Equation [14]. P_{atm} is regarded as the inner atmospheric pressure (1 bar = 14.50 MPa), and k is the ideal gas specific heat ratio obtained from the calculation of C_p.

$$P_{trans} = P_{atm}\left(\frac{k+1}{2}\right)^{\frac{k}{k-1}} \quad (14)$$

After obtaining the value of P_{trans}, the leak rate (W_n) is determined using Equation [15]. The discharge hole coefficient C_d has a value of 0.9, C_2 is a conversion factor with a value of 1, P_s is the equipment pressure, and T_s is the storage temperature in Kelvin. The gas constant R has a value of 8.314 kg/mol·K. G_c, which is the constant gravity, is equivalent to 9.81 m/s^2. A_n denotes the area of each leak hole, which is calculated using Equation [16].

$$W_n = \frac{Cd}{C2} \cdot A_n \cdot P_s \sqrt{\left(\frac{k \cdot MW \cdot gc}{R \cdot Ts}\right)\left(\frac{2}{k+1}\right)^{\frac{k+1}{k-1}}} \quad (15)$$

$$A_n = \frac{\pi d_n^2}{4} \quad (16)$$

Table 4. Representative fluids.

Fluid	MW (kg/m^3)	Eq. for C_p	AIT (Kelvin)
$C_3 - C_4$	817	Note 1	642

DOI: http://doi.org/10.17509/ijost.v7i1.42916
p- ISSN 2528-1410 e- ISSN 2527-8045

2.3.4. Available fluid mass analysis in gas leaks ($mass_{avail}$)

The RBI API provides an evaluation used to determine the consequences of equipment failure. This evaluation incorporates the presence of other equipment that contribute to an increase in the mass of the released fluid and is completed by calculating the mass of fluid available at the gas leak ($mass_{avail}$). This involves several steps, including determining the mass of the fluid ($mass_{comp}$) from the analyzed components, the fluid mass of each component in the inventory group ($mass_{comp}$,i), the mass of fluid in the inventory group ($mass_{inv}$), the flow rate for a diameter of 203.2 mm, the mass of the fluid added ($mass_{add}$,n), and the mass available at the leak.

1) Fluid mass ($mass_{comp}$) of the components analyzed

The fluid mass is calculated using Equation (17), where ρ is the density of the chosen representative fluid, and V is the volume of the tank (Equation [17]).

$$mass_{comp} = \rho \cdot V \cdot 50\% \quad (17)$$

2) Fluid mass of each component in the group inventory ($mass_{comp}$,i)

A fluid analysis for each component in the inventory group ($mass_{comp}$,i) was performed when there was a need to inspect a tank, and the fluid mass for each component was added. The measured tank has a value of 1, while the mass of fluid in the inventory group ($mass_{inv}$) is equivalent to the mass of the fluid ($mass_{comp}$) in the analyzed components. The mass of fluid in the inventory group is calculated using Equation [18].

$$\sum mass_{inv} = \sum mass_{scomp} \quad (18)$$

3) Flow rate for a diameter of 203.2 mm (8 in) (W_{max8})

The flow rate for a 203.2 mm in diameter (W_{max8}) is compared with the leak holes of 6.35, 25.4, 101.6, and 406.4 mm. The flow rate for 203.2 mm in diameter is obtained using Equation [19].

$$W_{max8} = \frac{Cd}{C2} \cdot A_n \cdot P_s \sqrt{\left(\frac{k \cdot MW \cdot gc}{R \cdot Ts}\right)\left(\frac{2}{k+1}\right)^{\frac{k+1}{k-1}}} \quad (19)$$

4) Calculation of mass of fluid added ($mass_{add}$,n)

Each inlet size increased the mass of the fluid in the equipment for 3 min. The mass of fluid added ($mass_{add,n}$) is determined using Equation [20].

$$mass_{add,n} = 180 \cdot min\,(W_n, W_{max8}) \quad (20)$$

5) Available mass on leak ($mass_{avail,n}$)

The available mass at the leak ($mass_{avail}$) is calculated using Equation [21], which is an analysis of the mass of the LPG when a leak occurs. This equation is obtained from the sum of the mass of LPG in the tank (Equation 18) and the mass addition of LPG leaking for 3 min ($\text{mass}_{\text{add,n}}$) by Equation [20]. This involves the mass of fluid ($mass_{comp}$) and the mass of fluid added ($mass_{add,n}$) as stated in Equation [20]. The available mass on the leak simulates the mass of the LPG in the tank and the mass of the LPG added to the "n" diameter. According to the API standard, the diameters used in calculating the RBI are 6.35, 25.4, 101.6, and 406.4 mm. The calculation of the diameter “n” is completed in a similar manner from the calculation of the mass of fluid added.

$$mass_{avail}, n = min\,(mass_{comp} + mass_{add,n}) \quad (21)$$

DOI: http://doi.org/10.17509/ijost.v7i1.42916
p- ISSN 2528-1410 e- ISSN 2527-8045

Table 5. Diameter of leak holes.

Release hole number	Release hole size	Range of hole diameter (mm)	Release hole diameter, d_n (mm)
1	Small	0 – 6.35	d_1 = 6.35
2	Medium	0.6.35 – 50.8	d_2 = 25.4
3	Large	50.8 – 152.4	d_3 = 101.6
4	Rupture	> 152.4	d_4 > 406.4

2.3.5. Determining the leak type

The RBL provides two leak- or release-type models to determine the dispersion method and its consequences. The instantaneous release is described as a momentary gas release (puff release). It occurs rapidly, thereby causing the liquid to spread out like a large cloud or pool. Continuous release (plume release) occurs for a longer time period, thereby allowing the liquid to disperse in an elongated ellipse (depending on weather conditions). The duration of each release hole size t_n is calculated using Equation [22].

$$t_n = \frac{C_3}{W_n} \quad (22)$$

2.3.6. Detection and isolation system

Generally, this industry has a variety of detection, isolation, and mitigation systems designed to reduce the leak effects of hazardous fluids. A simple method for assessing the effectiveness of various types of these systems is provided by the RBI API. The impact of the equipment's detection and isolation systems is determined by classifying them according to the actual conditions.

Furthermore, the leak reduction factor ($fact_{di}$) and the total time for each leak hole ($ld_{max,n}$) are determined after classifying the detection and isolation systems.

2.3.7. Rate calculation ($Rate_n$) and mass leaks ($Mass_n$) for the consequence analysis

The continuous leak type is determined by modeling a steady-state plume. Therefore, the leak rate (kg/s) and mass are used as inputs for the consequence analysis. The continuous release leak rate is obtained using Equation [23]. In addition, the leak mass is calculated using Equation [24]. The duration time (Id_n) is defined as the period of LPG leak in seconds.

$$Rate_n = W_n\,(1 - fact_{di}) \quad (23)$$

$$mass_n = min[(rate_n \cdot Id_n), mass_{avail\,n}] \quad (24)$$

2.3.8. Calculation of the explosion consequences

The procedure for calculating the effects of fire outbreaks and explosions involves several stages, namely, determining the reduction factor to mitigate the effects of the area ($fact_{mit}$) and the energy efficiency correction factor ($Eneff_n$).

1) Determination of area consequence mitigation reduction factors ($fact_{mit}$)

This factor is obtained as presented in **Table 6**.

2) Amount of the energy efficiency factor ($Eneff_n$)

The energy efficiency factor is calculated as shown in Equation [25].

$$Eneff_n = 4log_{10}(C_4 \cdot Mass_n) - 15 \quad (25)$$

2.3.9. Area consequences

An analysis of the consequences of the component damage area and personnel injury (injury damage) needs to be completed with the instantaneous or continuous blending factor value, AIT blending factor, mixture continuous or instantaneous consequence area, and final consequence value of the LPG storage tank. The analysis used Equations [26]-[43].

DOI: http://doi.org/10.17509/ijost.v7i1.42916
p- ISSN 2528-1410 e- ISSN 2527-8045

Table 6. Setting fire consequences for mitigation.

Mitigation system	Consequence area settings	Consequence area reduction factor
Inventory blowdown, coupled with isolation system classification B or higher	Reduce consequence area by 25%	0.25
Firewater deluge system and monitors	Reduce consequence area by 20%	0.20
Firewater monitors only	Reduce consequence area by 5%	0.05
Foam spray system	Reduce consequence area by 15%	0.15

$$CA_{cmd,n}^{AINL-CONT} = a(rate_n)b \cdot (1 - fact_{mit}) \quad (26)$$

$$CA_{cmd,n}^{AINL-INST} = min[\{a\,(Mass_n)b\}, C7] \cdot (1 - f_{actmit} / eneffn) \quad (27)$$

$$CA_{cmd,n}^{AIL-CONT} = a(rate_n)b \cdot (1 - fact_{mit}) \quad (28)$$

$$CA_{cmd,n}^{AINL-INST} = min[\{a\,(Mass_n)b\}, C7] \cdot (1 - fact_{mit} / eneffn) \quad (29)$$

$$CA_{inj,n}^{AINL-CONT} = [a\,x\,(effrate_n^{AINL-CONT})^b] \cdot (1 - fact_{mit}) \quad (30)$$

$$CA_{inj,n}^{AIL-CONT} = [a\,x\,(effrate_n^{AIL-CONT})^b] \cdot (1 - fact_{mit}) \quad (31)$$

$$CA_{inj,n}^{AINL-INST} = [a\,x\,(effrate_n^{AINL-INST})^b] \cdot \left(1 - \frac{fact_{mit}}{effrate_n}\right) \quad (32)$$

$$CA_{inj,n}^{AIL-INST} = [a\,x\,(effrate_n^{AIL-INST})b] \cdot (1 - \frac{fact_{mit}}{effrate_n}) \quad (33)$$

$$fact_n^{IC} = \frac{rate_n}{C_5} \quad (34)$$

$$fact_n^{IC} = 1.0 \quad (35)$$

$$CA_{cmd,n}^{AIL} = CA_{cmd,n}^{AIL-CONT} \cdot fact_n^{IC} + CA_{cmd,n}^{AIL-INST} \cdot (1 - fact_n^{IC}) \quad (36)$$

$$CA_{inj,n}^{AIL} = CA_{inj,n}^{AIL-CONT} \cdot fact_n^{IC} + CA_{inj,n}^{AIL-INST} \cdot (1 - fact_n^{IC}) \quad (37)$$

$$CA_{cmd,n}^{AINL} = CA_{cmd,n}^{AINL-CONT} \cdot fact_n^{IC} + CA_{cmd,n}^{AINL-INST} \cdot (1 - fact_n^{IC}) \quad (38)$$

$$CA_{inj,n}^{AINL} = CA_{inj,n}^{AINL-CONT} \cdot fact_n^{IC} + CA_{inj,n}^{AINL-INST} \cdot (1 - fact_n^{IC}) \quad (39)$$

$$CA_{cmd,n}^{flam} = CA_{cmd,n}^{AIL} \cdot fact^{AIT} + CA_{cmd,n}^{AINL} \cdot (1 - fact^{AIT}) \quad (40)$$

$$CA_{inj,n}^{flam} = CA_{inj,n}^{AIL} \cdot fact^{AIT} + CA_{inj,n}^{AINL} \cdot (1 - fact^{AIT}) \quad (41)$$

DOI: http://doi.org/10.17509/ijost.v7i1.42916
p- ISSN 2528-1410 e- ISSN 2527-8045

$$CA_{cmd,n}^{flam} = \left(\frac{\sum_{n=1}^{4} gff_n \cdot CA_{cmd,n}^{flame} \cdot}{gff_{total}} \right) \quad (42)$$

$$CA_{inj,n}^{flam} = \left(\frac{\sum_{n=1}^{4} gff_n \cdot CA_{inj,n}^{flame} \cdot}{gff_{total}} \right) \quad (43)$$

1) Area consequences of component damage

This factor is obtained in four stages: determining the consequences of the component damaged area for auto-ignition not likely continuous-release (AINL-CONT), auto-ignition not likely instantaneous release (AIL-INST), auto-ignition likely continuous-release (AIL-CONT), and auto-ignition likely instantaneous release (AIL-INST). The components AINL-CONT, AIL-INST, AIL-CONT, and AIL-INST are determined using Equations [26], [27], [28], and [29], respectively.

2) Area consequences of personnel injury (injury damage)

This factor is divided into four stages, including the consequences of personnel injuries AINL-CONT, AIL-CONT, AINL-INST, and AIL-INST, which are obtained using Equations [30], [31], [32], and [33], respectively.

3) Instantaneous/continuous blending factor values

The continuous blending factor ($fact_n^{IC}$) for each leak hole size is calculated using Equation [34]. In addition, the instantaneous blending factor is obtained by Equation [35].

4) AIT blending factor ($fact^{AIT}$)

The AIT blending factor value is based on three conditions.

a) Value $T_s + C_6 \leq$ AIT, then ($fact^{AIT}$) = 0.
b) Value $T_s - C_6 \geq AIT$, then ($fact^{AIT}$) = 1.
c) Value $T_s + C_6 >$ AIT $> T_s - C_6$, then $(fact^{AIT}) = \frac{T_s - AIT + C_6}{2.C_6}$

T_s is the temperature, C_6 has a value of 100 MW, while AIT is based on the fluid used in the study.

The next process after determining ($fact^{AIT}$) is finding the area consequence value of the continuous or instantaneous mixture using Equations [36], [37], [38], and [39].

5) Fire consequences of each hole (AIT blended)

The fire consequences of each hole (AIT blended) are determined using Equations [40] and [41].

6) Final value consequences of LPG storage tank

The analyzed component damage and personnel injury are used to calculate the final value of the LPG storage tank consequences, as stated in Equations [42] and [43].

2.4. Determination of Risk Level

In general, the risk level is obtained by analyzing the results of the consequence of failure (*CoF*) and the probability of failure (*PoF*). This is further displayed in a 5 × 5 matrix, as shown in **Table 7**. The matrix displays low, medium, medium-high, and high-risk levels based on the category of possible failures. The main result of the RBL method is a matrix that places the tool at a certain level of risk. Therefore, appropriate and accurate recommendations are required.

2.5. Determine the Inspection Schedule

API 510 states that pressure vessels need to be inspected internally or on-stream for a maximum of 10 years or until it has reached

DOI: http://doi.org/10.17509/ijost.v7i1.42916
p- ISSN 2528-1410 e- ISSN 2527-8045

half of their remaining life, which is usually less. This value is considered in this study because the LPG storage tanks are located on a tropical island with high humidity, above 80% on average. The remaining life is determined using Equation [44].

$$Remaining\ life = \frac{t_{actual} - t_{required}}{corrosion\ rate} \quad (44)$$

However, assuming that the remaining life value of the equipment is less than four years, the inspection interval is the complete remaining life or a maximum of two years. In addition, external inspections of pressure vessels need to be carried out every 5 years.

3. CASE STUDY

We conducted a case study to verify the performance of the RBL analysis on LPG tanks at a gas distributor company in Magelang City, Indonesia. The locations are shown in **Figure 3**. The wall thickness data related to the LPG storage tanks were obtained using an ultrasonic thickness gauge. Furthermore, the working temperature was determined using an infrared thermometer material. The LPG storage tank specifications used in this study are listed in **Table 8**. A photographic view of the LPG tank is presented in **Figure 4**. The main components of LPG include 68% butane, 30% propane, 2% pentane, and insignificant amounts of other components. Applications have several subsystems. In creating an application system, integrated information design that provides information on how the system functions are required. This is implemented using data flow diagrams (DFD), and the results of the designed application system are shown in **Figure 5.**

The data collection process related to the wall thickness of the LPG storage tank is divided into two areas: (i) the spot head and (ii) the shell.

The spot head has two sides, right and left, while the shell is divided into six areas, shells I, II, III, IV, V, and VI. Each was divided into ten inspection points. The spot shell and head were positioned at three corner points, namely 90, 180, and 270°. The spot head had the smallest thickness of 20.1 mm. Shell VI had the safest wall thickness (19.5 mm) and an inspection point positioned at 180°. Shell IV needed attention because it had a thickness of 18.9 mm at a 180° inspection point. It had the smallest value of all the shells. The results of the thickness measures of the LPG storage tank are presented in **Figure 6**.

Table 7. Categories of possible failure and consequences of failure.

Possible failure		Consequences of failure	
Category	**Range**	**Category**	**Range (m^2) pp**
1	*Df-total R* ≤2	A	*CA* ≤ 9.29
2	2 ≤ *Df-total R*≤20	B	9.29 ≤ *CA* ≤ 92.9
3	20 ≤ *Df-total R*≤100	C	92.9 ≤ *CA* ≤ 278.7
4	100 ≤ *Df-total R* ≤1000	D	278.7 ≤ *CA* ≤ 929
5	*Df-total R*≥ 1000	E	*CA* ≥ 929

DOI: http://doi.org/10.17509/ijost.v7i1.42916
p- ISSN 2528-1410 e- ISSN 2527-8045

Table 8. Specifications for LPG storage tanks.

Item		Specification
Pressure vessel type	:	LPG storage tank capacity 50 ton
Type	:	Horizontal
Temperature design	:	55 °C
Dimension	:	2890 mm (ID) x 15000 mm (S/S)
Inside radius (R_i)	:	1448 mm
Material	:	SA 516 Grade 70
Year built/used	:	2010
Inside diameter	:	2895 mm
Pressure	:	1.38 MPa

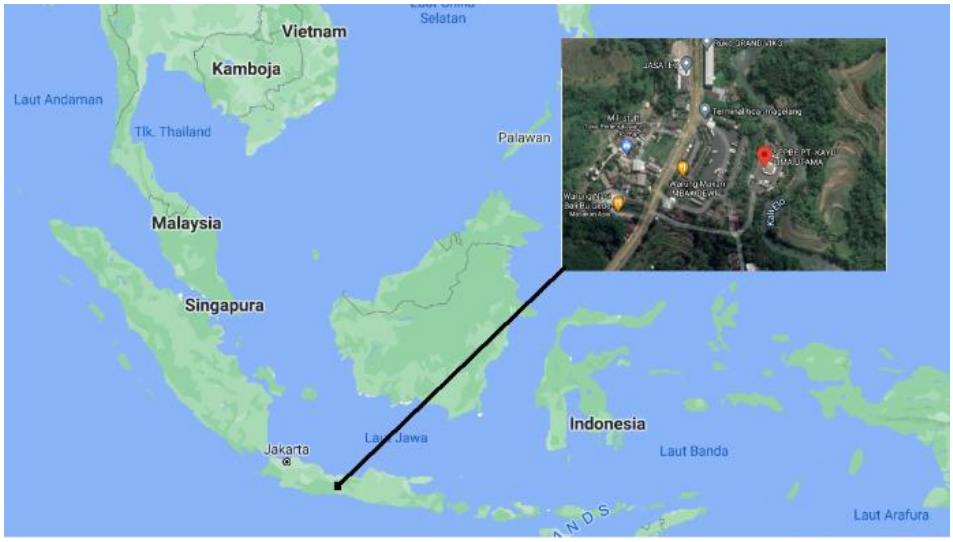

Figure 3. Research location.

Figure 4. Photographic view of the LPG tank studied in PT Kayu Lima Utama gas station.

DOI: http://doi.org/10.17509/ijost.v7i1.42916
p- ISSN 2528-1410 e- ISSN 2527-8045

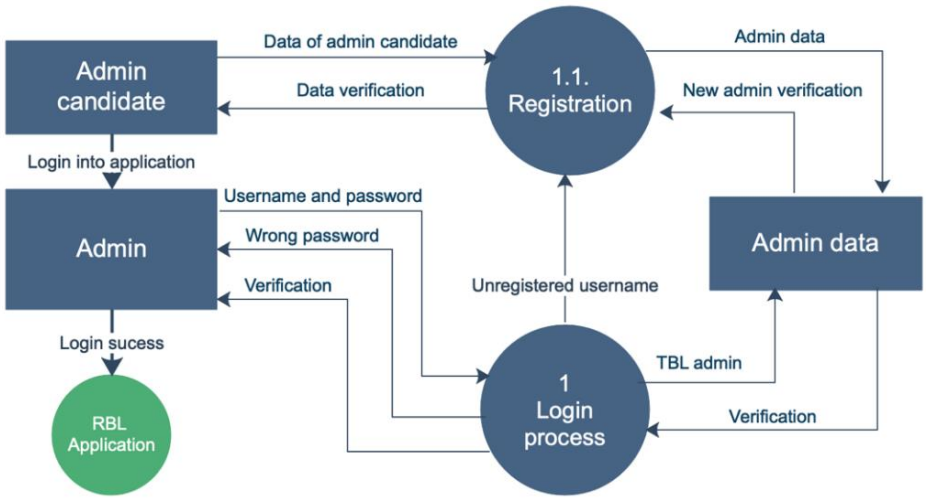

Figure 5. The data flow diagram of the designed application system.

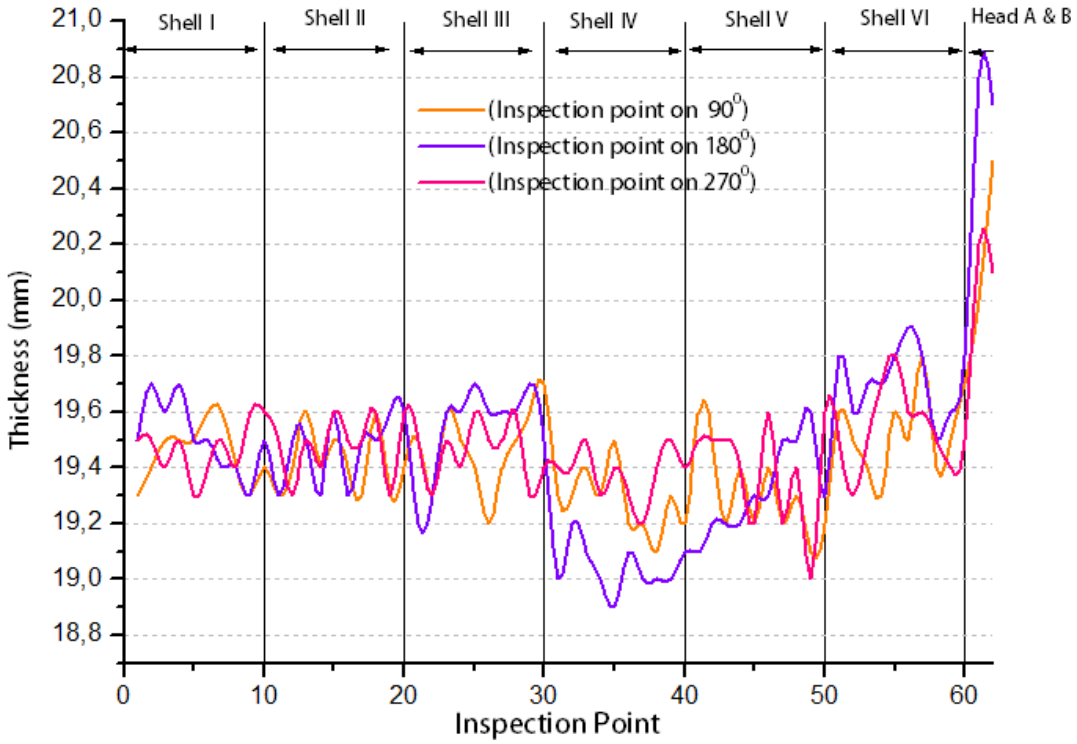

Figure 6. The data thickness of the LPG storage tank wall.

Then, the data were inputted into the application that was designed for an analysis based on the RBL method. Furthermore, the age gap between the inspection carried out and the previous one was one year, as determined by Equation [3].

The measured thicknesses of the LPG storage tank were analyzed and compared with previous measurements. This method served as a reference for determining the short-term corrosion rate. The comparison results were used to obtain information on all the examined spots and shell II, which had a

DOI: http://doi.org/10.17509/ijost.v7i1.42916
p- ISSN 2528-1410 e- ISSN 2527-8045

significant thickness difference. Shell II exhibited more corrosion than did the other areas. These data show that each shell had a different amount of corrosion. A comparison of the LPG storage tank test results with the previous inspection is shown in **Figure 7**. This test is a comparison of the last data obtained from the historical inspection data.

Some information is obtained based on a comparative evaluation of the wall thickness and analysis of short-term corrosion rates. Shells II and I have the highest and lowest short-term corrosion rates, respectively. Shell II must be prioritized when investigating corrosion hazards. The short-term corrosion rate analysis was carried out using Equation [4], and the results are shown in **Figure 8**.

The long-term corrosion rate was calculated using Equation [5]. The analysis results show the largest value of 0.041 mm/y on shell V and 0.15 mm on head A. After discerning the corrosion rate, the next process was to determine the minimum thickness (T_{min}) on the spotted shell and head using Equations [6] and [7], respectively. The values of T_{min} on the spot shell and head were 14.53 mm/y, and 14.47 mm/y, respectively. The difference between the wall thickness of the spotted shell and T_{min} was 4.37 mm. This value indicates the need to be aware of the dangers of corrosion and cracking. However, the dangers arising from external factors must also be considered.

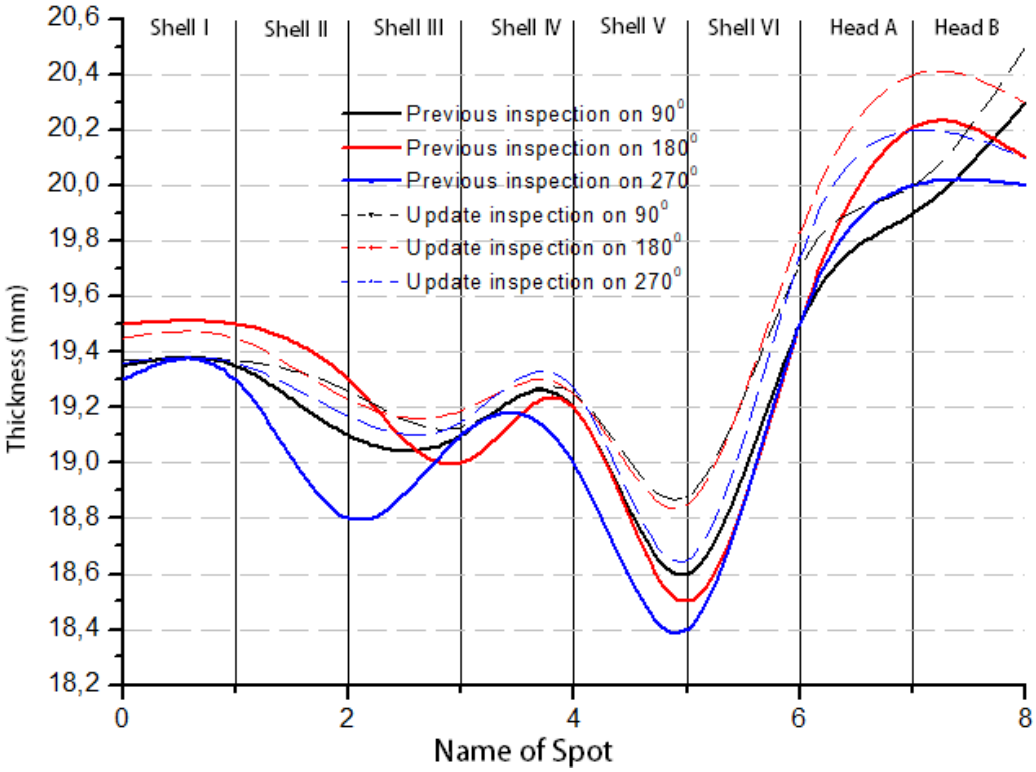

Figure 7. Comparison of the smallest data thickness from the previous inspection period to the current one.

DOI: http://doi.org/10.17509/ijost.v7i1.42916
p- ISSN 2528-1410 e- ISSN 2527-8045

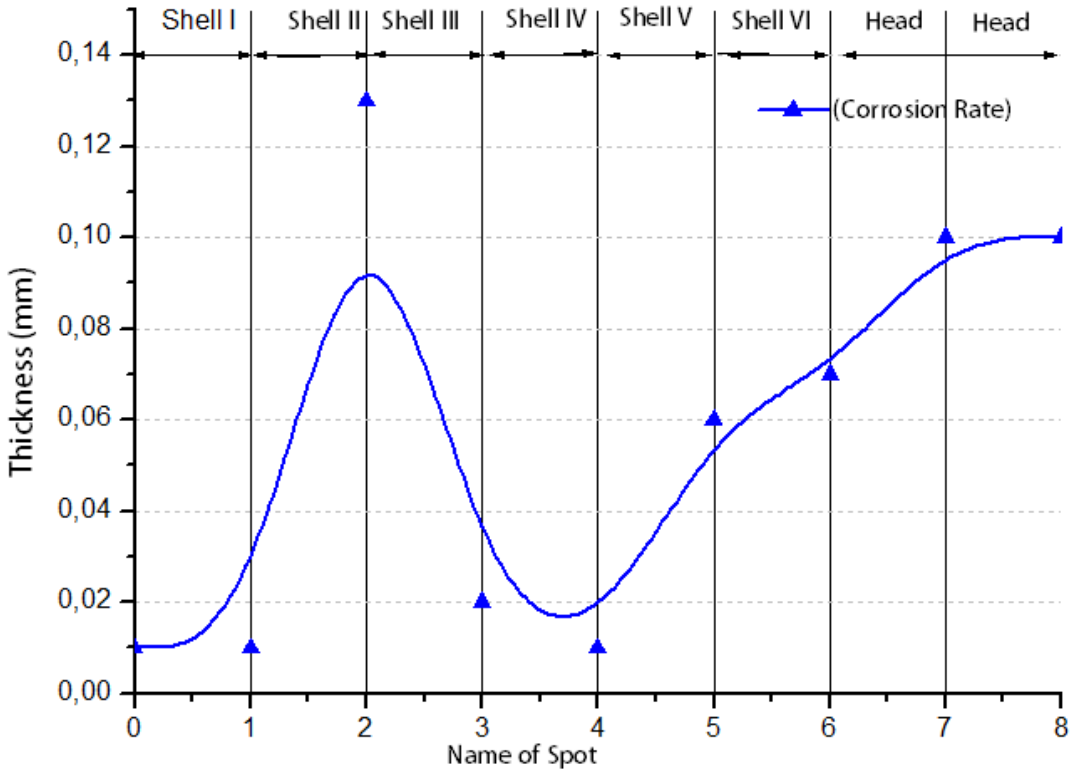

Figure 8. The calculated results of the short corrosions rate of the LPG storage tank.

4. RESULTS AND DISCUSSION

4.1. PoF Analysis Results

The analysis of the *PoF* in accordance with the observed equipment is denoted as $(P_f(t))$, which is based on Equation (2) and has three variables. These are the common failure frequency variable (*gff*), the damage factor $(D_f(t))$, and management system factor (F_{MS}).

4.1.1. Common failure frequency values (gff)

According to the API standard, the common failure frequency values (gff) of the LPG storage tank were 3.06 × 10^{15} failures/y. These common failure frequencies are assumed to have a log-normal distribution, with error rates ranging from 3% to 10%.

4.1.2. Damage factor $(D_f(t))$

The damage factor $(D_f(t))$ is a *PoF* variable. Based on the previous analysis, the audited effectiveness was in category B (usually effective). This is because over 50% of the ultrasonic thickness measurements were carried out on all LPG storage tank parts.

4.1.3. Thinning damage factor ($D_f$thin)

After determining the category of the examined effectiveness, the next step was to discern the value of the damage factor thinning (Df^{thin}). However, this required additional factors, including the injection or mix point (F_{IP}), dead legs (F_{DL}), welded construction (F_{WD}), tank maintenance per API 653 (F_{AM}), settlement (F_{SM}), and online monitoring (F_{OM}). The pressure vessel was used to analyze the additional factors according to its structure, construction, maintenance, monitoring conditions, etc.

DOI: http://doi.org/10.17509/ijost.v7i1.42916
p- ISSN 2528-1410 e- ISSN 2527-8045

The injection or mix point (F_{IP}) is an additional factor in pipeline systems. This study case did not include a pipe network; therefore, the F_{IP} value was 1. The dead legs (F_{DL}) is a pipe component that is only used at startup or shutdown. Because the system, in this case, did not include this component, the F_{DL} value was 1. Welded construction (F_{WD}), tank maintenance per API 653 (F_{AM}), and settlement (F_{SM}) are used for the analysis of atmospheric storage tanks. However, because a pressure vessel was used in this study, the values for F_{WD}, F_{AM}, and F_{SM} were 1. Finally, because the data collection was based on offline monitoring, its value was 1.

The next process was to determine the total thinning damage factor D_f^{thin} that occurred in the pressure vessel using Equation [9].

$$D_f^{thin} = \frac{1 \cdot 1 \cdot 1 \cdot 1 \cdot 1 \cdot 1}{1} = 1$$

The calculated results obtained a D_f^{thin} value of 1.

Equation [11] was used to obtain the p-score value of the management system factor, which was 50%. This was used to calculate F_{SM} based on Equation [12], and the final value was 1. The *PoF* value obtained from Equation [2] is as follows:

$$\begin{aligned} P_f(t) &= gff \cdot D_f(t) \cdot F_{MS} \\ &= (3.06 \times 10^{-5}) \cdot (1) \cdot (1) \\ &= 3.06 \times 10^{-5} \text{ failure/y} \end{aligned}$$

The risk determination, based on the *PoF* value combined with the effectiveness category, produced a B rating of 1. The risk of the LPG storage tank was low. The results of the risk analysis in accordance with *PoF* are shown in **Figure 9**.

4.2. Results of the CoF Analysis

The *CoF* analysis was conducted through eight calculation phases, which included the following.

4.2.1. Determination of the representative fluid

First, the representative fluid was selected and the stored fluid phase was determined. Fluids that have a vapor phase include several property variables, namely, the molecular weight (MW), ideal gas specific heat ratio (k), and auto-ignition temperature (AIT). The process of determining these two variables was carried out as in the aforementioned discussion, as stated in **Table 4**.

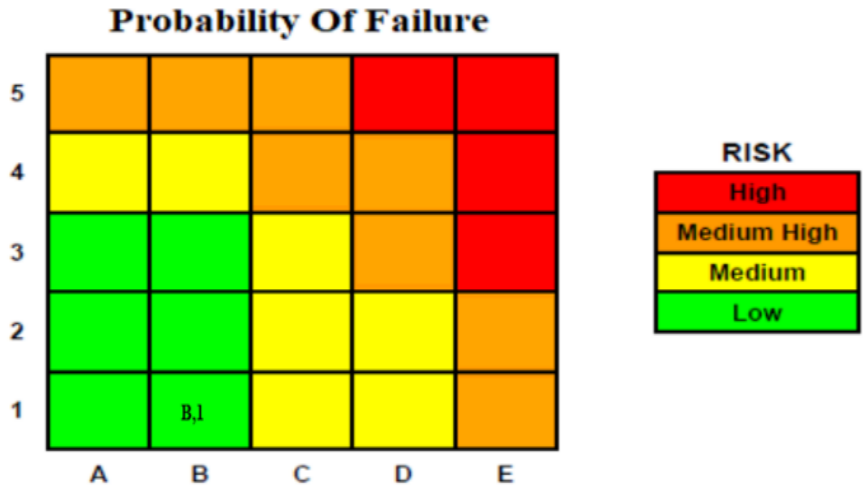

Figure 9. The results of the risk of LPG storage tank using *PoF* analysis.

DOI: http://doi.org/10.17509/ijost.v7i1.42916
p- ISSN 2528-1410 e- ISSN 2527-8045

The specific heat ratio for an ideal gas (k) is another variable for determining the representative fluid. Its magnitude is calculated based on the value of the constant pressure specific heat (C_p) which is obtained using Equation (12). A calculated result of -1.45×10^{10} J/mol·K was obtained by inputting the constant variables A (2.632), B (3.188×10^{-1}), C (1.347×10^{-1}) , D (1.466×10^{-8}), and T (55 °C/328.15 K). The value of k (0.99 J/mol·K) was found from Equation (13) in accordance with the variable R (8.314 J/mol·K) as the gas constant. The value of k was used to calculate the transition pressure (P_{trans}).

4.2.2. Selection of leak hole size

The release hole size was selected based on the type of equipment being observed and Part 3 of the API 581 Annex standard. According to the API standard, the leak hole size was included in the pressure vessel category. The selected sizes have four leak holes, from small (6.35 mm), medium (25.5 mm), large (101.4 mm), and rupture (406.4 mm), as shown in **Table 5**. The LPG storage tank used in this study had a size of 2890 mm. Therefore, the leak hole size was determined to be 406.4 mm.

4.2.3. Calculation of the leak rate (W_n)

The leak rate analysis includes several procedures. The equation used to determine (W_n) is based on the phase of the stored fluid. Subsequently, the transition pressure (P_{trans}) used to determine the tool's working pressure has a value that is either smaller or greater than the atmospheric pressure. This is determined using Equation [14]. The value of the transition pressure was used for the selection of equations to determine the leak rate. The calculated result (P_{trans}) for this device was 23.91 kPa.

First, the leak rate (W_n) was determined by locating the area of each leak hole (A_n) using Equation [16]. The calculated area of each leak hole is listed in **Table 9**. After obtaining each leak hole area, the next step was to determine (W_n) for each of them. This included small, medium, large, and rupture holes. The leak rate (W_n) was calculated using Equation [15]. A comparison of the results (W_n) between the holes is shown in **Figure 10**.

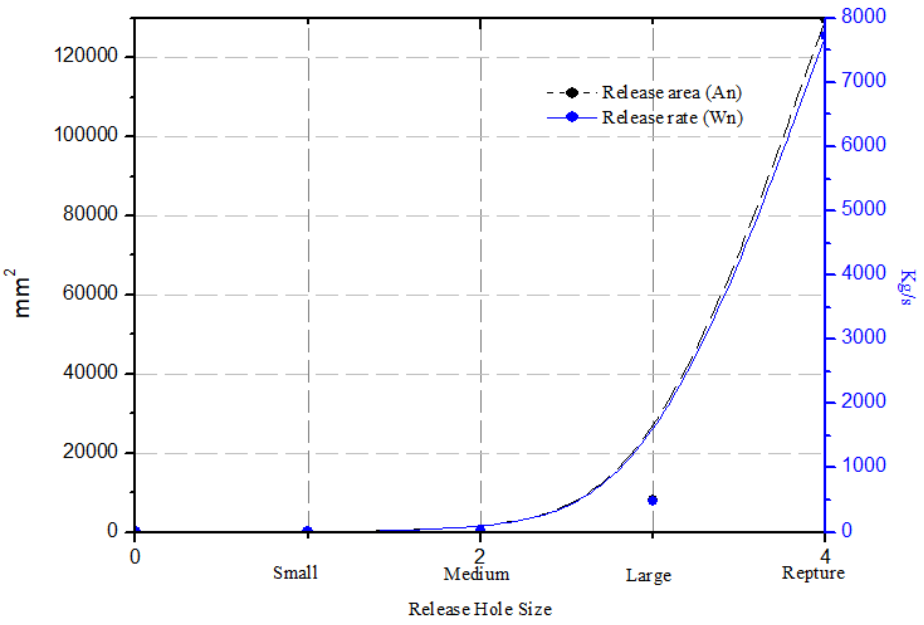

Figure 10. W_n comparison of LPG from each hole area.

DOI: http://doi.org/10.17509/ijost.v7i1.42916
p- ISSN 2528-1410 e- ISSN 2527-8045

4.2.4. Available fluid mass analysis in gas leaks ($M_{ass\ avail}$)

The API RBL provides information regarding the consequences of failure, which are evaluated in the presence of other equipment that contributes to the increase in the mass of components ($M_{ass\ comp}$) which is calculated using Equation [17]. The observed mass value of the LPG component was approximately 381 kg.

The total mass in the inventory group ($M_{ass\ inv}$) was calculated using Equation [18]. Assuming that the component being measured is only one component, then ($M_{ass\ inv}$) = ($M_{ass\ comp}$). In this study, the total mass ($M_{ass\ inv}$) was 381 kg in diameter of 203.2 mm (8 in) (W_{max8}). Although this diameter is not listed in **Table 9**, it was determined by comparing the leak holes. The fluid flow rate with a diameter of 203.2 mm (A=32,442.33 mm^2) was obtained using Equation (19). This calculation resulted in a W_{max8} of 1930 kg/s. Furthermore, Equation (20) was used to determine the fluid mass ($M_{ass\ add}$) and the resulting leak rate for each hole size when the leak duration was 3 min, as shown in **Table 10**.

The maximum available fluid mass value of each leak hole ($M_{ass\ avail}$) was determined using Equation [21]. The resulting analysis ($M_{ass\ avail}$) is presented in **Table 11**.

4.2.5. Determining the type of leak

There are two types of leaks: continuous and instantaneous. First, the time required to discharge a fluid weighing 4535.92 kg must be obtained before determining the type of leak using Equation (22). Subsequently, the type of leak for each hole must also be determined. The continuous type occurs when the leak size is > 6.35 mm or the time it takes to discharge 4535.92 kg of fluid is more than 3 min. However, if these criteria are not met, the type is categorized as instantaneous. The calculated result is presented in **Table 12**.

Table 9. The results of the calculated area of each leak hole.

Number	Release hole size	Release hole area, A_n (mm^2)	Release Rate, W_n (kg/s)
1	Small	A1 = 31.68	1.89
2	Meduim	A2 = 509.91	30.16
3	Large	A3 = 8,110.58	482.56
4	Reptune	A4 = 129,769.33	7720.98

Table 10. Calculation results ($M_{ass\ add}$).

Number	Fluid mass (kg)
Mass add 1	339.3
Mass add 2	5,428.8
Mass add 3	86,961
Mass add 4	347,444.1

Table 11. Calculation results ($mass_{avail}$).

Number	$mass_{avail}$ (kg)
$M_{ass\ avail1}$	381,470.3
$M_{ass\ avail2}$	386,559.8
$M_{ass\ avail3}$	467,991.9
$M_{ass\ avail4}$	728,575.1

DOI: http://doi.org/10.17509/ijost.v7i1.42916
p- ISSN 2528-1410 e- ISSN 2527-8045

Table 12. Results of determining the type of leakage.

No.	D_n	Time required to release 4,535.92 kg (s)	Release type
t1	6.35	2,406.32	Continous
t2	25.4	150.39	Instantaneous
t3	101.6	9.39	Instantaneous
t4	406.4	0.59	Instantaneous

4.2.6. Detection and isolation system

The detection and isolation system that emerged after being evaluated in the case study was in category B. The evaluation was carried out based on observations in the industry, following the API RBI standards. The release magnitude adjustment and reduction factor ($fact_{di}$) were determined by referring to the API standard. Based on this standard analysis, detection and isolation system B had a value ($fact_{di}$) of 0.15. Immediately after obtaining the grade ($fact_{di}$), the total leak time for each leak hole ($ld_{max,n}$) was determined. According to the API standards, the maximum duration of the leak in category B detection and isolation systems for equipment over 406.4 mm is rated as 10 min. Rate calculation and mass leaks for the analysis of the consequences

This analysis required the support of several variables, including the leak duration, release hole, and its number. In addition, each leak hole size was calculated after determining the rate value ($rate_n$), duration (ld_n), and mass leak ($mass_n$) using Equations [23] and [24]. The calculated results of ($rate_n$) and mass leak ($mass_n$) are listed in **Table 13.** The leak duration values for the small-type leaks were not calculated. This is because the study did not use the leak duration based on the detection and isolation system with a diameter of 6.35 mm.

Table 13. Determination results of the type of leakage.

Release hole number	Release hole size	Adjusted release rate, $rate_n$ (kg/s))	Leak duration, ld_n (s)	Release mass, $mass_n$ (kg)
2	Medium	25.8	1,800	46,440
3	Large	410.2	1,200	492,240
4	Rupture	6,562.8	600	3,937,680

4.2.7. Explosion consequences calculation

Several stages are involved in determining the consequences of a fire or explosion, such as discerning the value of the mitigation area consequence reduction factor ($fact_{mit}$) and energy efficiency correction factors ($Eneff_n$). The value of the consequence area mitigation reduction factor ($fact_{mit}$) refers to the API 581 standard. This standard states that the mitigation system adopted in the research media due to the fire was included in the category of "firewater deluge and monitor systems". This is because the LPG storage tank had a control room for detecting fire hazards. Therefore, the reduction factor reduced the consequence area ($fact_{mit}$), which had a value of 0.20. The energy efficiency correction factor ($Eneff_n$) of each leak hole size was calculated using Equation (25). The calculated results for determining the energy efficiency correction factor ($Eneff_n$) are listed in **Table 14**.

DOI: http://doi.org/10.17509/ijost.v7i1.42916
p- ISSN 2528-1410 e- ISSN 2527-8045

4.2.8. Area consequences

Each of the leak hole sizes was calculated based on two consequences: component damage and personnel injury. The area consequence of component damage has four conditions, including AINL-CONT, AINL-INST, AIL-CONT, and AIL-INST. These are determined using Equations [26], [27], [28], and [29], respectively.

The area consequence of personal injury also has four conditions, namely, AINL-CONT, AIL-INST, AIL-CONT, and AIL-INST. These are determined using Equations [30], [31], [32], and [33]. The constants for calculating the area consequences of component damage and personnel injury are listed in **Table 15.**

1) Area consequences of component damage

The fluids observed in this study fell into the $C_3 - C_4$ (Type 0) category. The calculated results of the component damages ($CA_{cmd,n}^{AINL-CONT}$) and ($CA_{cmd,n}^{AIL-CONT}$) in 6.35 mm holes are shown in **Tables 16** and **17**. The calculated area consequences of component damage ($CA_{cmd,n}^{AINL-INST}$) and ($CA_{cmd,n}^{AIL-INST}$) in holes of 25.4, 101.6, and 406.4 mm are shown in **Tables 18** and **19**, respectively.

2) Area consequences of personnel injury

The area consequence values of personnel injury $\left(CA_{inj,n}^{AINL-CONT}\right)$ in 6.35 mm holes are shown in **Tables 20** and **21**, respectively. Then, the area consequence values of personnel injury ($CA_{inj,n}^{AINL-INST}$) in holes of 25.4, 101.6, and 406.4 mm are shown in **Tables 22** and **23**, respectively.

Table 14. Calculation results ($Eneff_n$).

Hole Size	$Eneff_n$	Hole Size	$Eneff_n$
Small	1.000	Large	9.142
Medium	5.029	Reptune	12.754

Table 15. Constants for determining the area consequences of component damage and personnel injury.

Constant*	Area Consequences			
	AINL – CONT	AIL – CONT	AINL – INST	AIL – INST
A	49.48	313.60	27.96	522.90
B	1.00	1.00	0.72	0.63
a	125.20	836.70	57.72	1769.00
b	1.00	1.00	0.75	0.63

Note: A and B are for component damages; a and b are for personel injury

Table 16. Calculation results ($CA_{cmd,n}^{\mathrm{AINL-CONT}}$).

Hole Size	$CA_{cmd,n}^{\mathrm{AINL-CONT}}$	Effrate ($CA_{cmd,n}^{\mathrm{AINL-CONT}}$)
Small	138.469	3.532

Table 17. Calculated results ($CA_{cmd,n}^{\mathrm{AIL-CONT}}$).

Hole Size	$CA_{cmd,n}^{\mathrm{AIL-CONT}}$	$Effrate_n$ ($CA_{cmd,n}^{\mathrm{AIL-CONT}}$)
Small	138.469	3.532

Table 18. Calculation results ($CA_{cmd,n}^{\mathrm{AINL-INST}}$).

Hole size	$CA_{cmd,n}^{\mathrm{AINL-INST}}$	$Effrate_n$($CA_{cmd,n}^{\mathrm{AINL-INST}}$)
Medium	17,308.92	101,732.35
High	52,355.89	1,085,142.78
Reptune	167,715.12	8,681,142.23

DOI: http://doi.org/10.17509/ijost.v7i1.42916
p- ISSN 2528-1410 e- ISSN 2527-8045

Table 19. Calculated results ($CA_{cmd,n}^{\mathrm{AIL-INST}}$).

Hole size	$CA_{cmd,n}^{\mathrm{AINL-INST}}$	Eff_{rate} ($CA_{cmd,n}^{\mathrm{AINL-INST}}$)
Medium	11,8551.10	101,732.35
High	289,786.73	1,085,142.78
Reptune	769,851.63	8,681,142.23

Table 20. Calculation results ($CA_{inj,n}^{AINL-CONT}$).

Hole size	$CA_{inj,n}^{\mathrm{AIL-CONT}}$	$effrate_n$ ($CA_{inj,n}^{\mathrm{AIL-CONT}}$)
Small	353.24	3.53

Table 21. Calculated results ($CA_{inj,n}^{\mathrm{AIL-CONT}}$).

Hole size	$CA_{inj,n}^{\mathrm{AIL-CONT}}$.	$effrate_n$ ($CA_{inj,n}^{AIL-CONT}$)
Small	2,362.45	3.53

Table 22. Calculated results ($CA_{inj,n}^{\mathrm{AINL-INST}}$).

Hole size	$CA_{inj,n}^{\mathrm{AINL-INST}}$	$effrate_n$ ($CA_{inj,n}^{\mathrm{AINL-INST}}$)
Medium	51,642.22	101,732.14
High	167,703.17	1,085,142.78
Reptune	571,795.34	8,681,142.23

Table 23. Calculation results ($CA_{inj,n}^{\mathrm{AIL-INST}}$).

Hole size	$CA_{inj,n}^{\mathrm{AIL-INST}}$	$effrate_n CA_{inj,n}^{\mathrm{AIL-INST}}$
Medium	401,756.51	101,732.14
High	982,055.05	1,085,142.78
Reptune	2,608,941.65	8,681,142.23

3) Instantaneous/continuous blending factor values

The instantaneous or continuous blending factor ($fact_n^{IC}$) for each leak hole size was determined according to Equation (34). The calculated result ($fact_n^{IC}$) in each hole size was less than 1 and included in the continuous category. However, if the value was greater than 1, it was included in the instantaneous category. The calculated results are presented in **Table 24**.

4) AIT blending factor ($fact^{AIT}$)

The AIT blending factor ($fact^{AIT}$) was obtained by inputting a Ts value of 328.15 K and AIT 642.35 K. It was discovered that the value of Ts + C6 was smaller than that of AIT; therefore, ($fact^{AIT}$) was equal to 0. The consequential area of the continuous or instantaneous mixture was obtained by determining the value of the AIT blending factor.

5) Fire every hole (AIT Blended)

The fire per hole (AIT blended) was calculated after determining the consequence area of the continuous or instantaneous mixture. The results of the fire consequences ($CA_{cmd,n}^{flam}$) and ($CA_{inj,n}^{flam}$) in each hole are shown in **Table 25**.

This was determined by adding all the consequence area values for each hole. The result of this calculation was divided by the total generic failure frequency (total *gff*). The system automatically calculated the final consequence value of the LPG storage tank,

DOI: http://doi.org/10.17509/ijost.v7i1.42916
p- ISSN 2528-1410 e- ISSN 2527-8045

after which the final consequence value in the "CA end of flam $_{cmd}$ TOTAL" and "CA end of flam $_{inj}$ TOTAL" were displayed (**Table 26**).

The analysis of the failure in this study only included the consequences of fire and explosion. The final value was determined using the highest fire and explosion score, which was 2381.3 m^2. This was obtained from the final consequences of personal injury.

4.3. Risk Level Determination

The risk value of the tool was obtained by multiplying *PoF* and *CoF*, resulting in 0.073 failure/y·m^2. The *PoF* calculation was used to obtain a value of 1 for Df_{total}. According to the *PoF* category, Df_{total} had a value of ≤ 2. These calculations were used to determine the low probability value of the failure. This is because the corrosion rate was low, and the thickness of the tool was still far from its minimum. Meanwhile, the CA value of the final *CoF* was 2381.3 m^2. This value was included in the COD category at level E; therefore, the CA was > 929 m^2. The CoF calculation has an extremely high value (medium-high). This condition is due to the type of fluid contained in the LPG storage tank, which was dangerous and flammable. Furthermore, the fluid flow in the tool was also high. The results of the *PoF* and *CoF* analyses are shown in **Figure 11**, which also shows that the LPG storage tanks had a medium-high level of risk. Therefore, there is a need for supervision and inspection to ensure that the equipment safety system operates effectively.

4.4. Scheduling

According to API 510, the pressure vessel needs to be inspected internally or on-stream for a maximum of 10 years or when it has reached half of its remaining life, whichever value is lower; Equation [35] is used to determine the remaining age. The results of the remaining life calculations are listed in **Table 27**.

The calculated results in **Table 27** show that the remaining life in the LPG storage tank was 33.5 years, which was the lowest value. Therefore, an external inspection of the pressure vessel needs to be carried out within a maximum of five years because the remaining life of the LPG storage tank is over 10 years. Therefore, the next inspection for the LPG storage tank will be scheduled for 2025. Moreover, the inspection interval was every 5 years.

Table 24. Blending factor ($\mathrm{fact}_{\mathrm{n}}^{\mathrm{IC}}$).

Hole size	Blending factor
Small	0.064
Medium	1
High	1
Reptune	1

Table 25. Calculation results ($CA_{cmd,n}^{flam}$) and ($CA_{inj,n}^{flam}$).

Hole size	$CA_{cmd,n}^{flam}$	$CA_{inj,n}^{flam}$
Small	129.67	330.79
Medium	17,308.92	51,642.22
High	52,355.89	167,703.17
Reptune	167,715.12	571,795.34

Table 26. CA final results for component damage and personnel injury.

Final component damage consequence areas **(CA flam $_{cmd}$ TOTAL)**	***Final personnel injury consequence areas,*** **(CA flam $_{inj}$ TOTAL)**
731.4 m^2	2,381.3 m^2

DOI: http://doi.org/10.17509/ijost.v7i1.42916
p- ISSN 2528-1410 e- ISSN 2527-8045

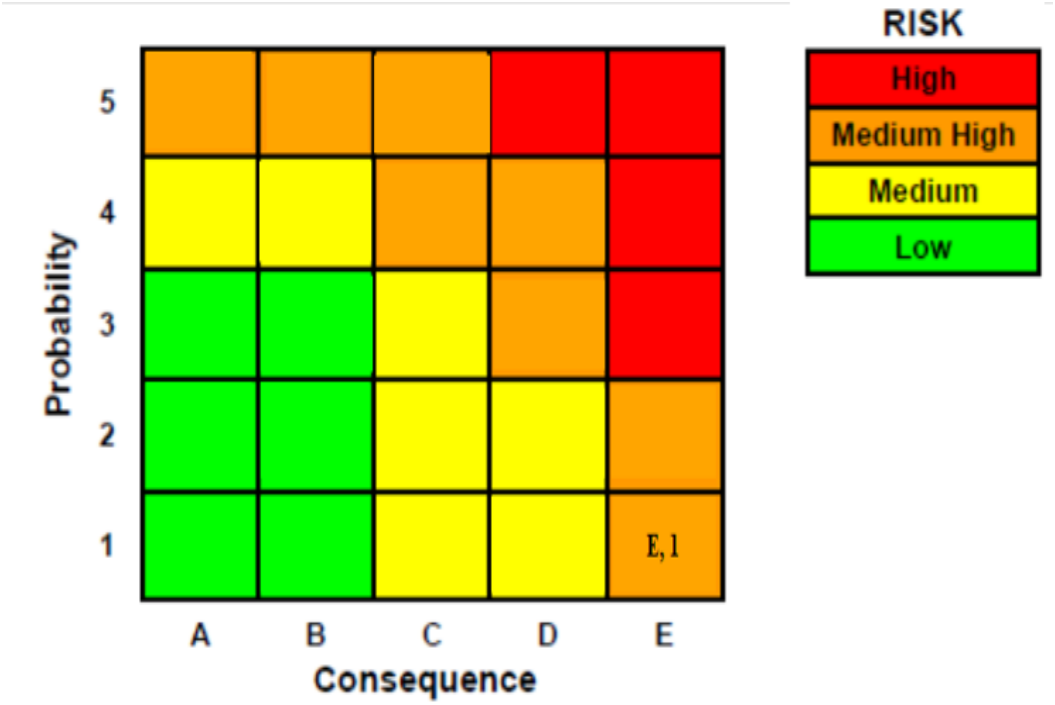

Figure 11. The results of the risk level calculation.

Table 27. The results of the remaining life calculation.

Description	Short Rly	Long Rly
Remaining Life Shell	81.154	98.968
Remaining Life head	50.221	33.481

5. CONCLUSION

Based on the data analysis, several conclusions can be drawn. The risk level of the LPG container tank analyzed was high (medium-high risk) with a probability of failure (*PoF*) in category 1, while the total value of D_f was 1. The *CoF* was in category E with a CA value of 2381.3 m^2. Based on this level of inspection, the tank needs to be closely supervised. The remaining life of the LPG storage tank was 33.5 years. According to the RBI API, external inspections need to be carried out every five years. A subsequent examination was recommended in 2025. In this study, the qualitative RBI method was used. However, for further research, it is advisable to determine an examination schedule using the quantitative RBI method to obtain accurate results. The applications created in this study were used on computers with certain types of operating systems. Further research is recommended to develop applications for various types of operating systems.

6. ACKNOWLEDGEMENTS

The authors are grateful to Universitas Muhammadiyah Magelang for funding this research and to PT Kayu Lima Utama for the research facility.

7. AUTHORS' NOTE

The authors declare that there is no conflict of interest regarding the publication of this article. The authors confirmed that the paper was free of plagiarism.

DOI: http://doi.org/10.17509/ijost.v7i1.42916
p- ISSN 2528-1410 e- ISSN 2527-8045

8. REFERENCES

Abubakirov, R., Yang, M., and Khakzad, N. (2020). A risk-based approach to determination of optimal inspection intervals for buried oil pipelines. *Process Safety and Environmental Protection, 134*, 95-107.

Bariha, N., Mani, I., and Chandra, V. (2016). Fire and explosion hazard analysis during surface transport of liquefied petroleum gas (LPG): A case study of LPG truck tanker accident in Kannur, Kerala, India. *Journal of Loss Prevention in the Process Industries, 40*, 449–460.

Bhatia, K., Khan, F., Patel, H., and Abbassi, R. (2019). Dynamic risk-based inspection methodology. *Journal of Loss Prevention in the Process Industries, 62*, 103974.

Chang, J. I., and Lin, C. (2006). A study of storage tank accidents. *Journal of Loss Prevention in the Process Industries, 19*(1), 51–59.

Fauziah, N. R., Maoludin, S. A., Ramadhan, W. S., Wafi, W., Khoerunnisa, F., Winarno, N. (2021). Geothermal: From education to a new solution for renewable energy. *Indonesian Journal of Multidiciplinary Research, 1*(1), 85-88.

Gallab, M., Bouloiz, H., Alaoui, Y. L., and Tkiouat, M. (2019). Risk assessment of maintenance activities using fuzzy logic*. Procedia Computer Science, 148*, 226-235.

Hidayah, F., Muslihah, F., Nuraida, I., Winda, R., Vania, V., Rusdiana, D. and Suwandi, T. (2021). Steam power plant powered by wood sawdust waste: A prototype of energy crisis solution. *Indonesian Journal of Teaching in Scienc*e, *1*(1), 39-46.

Irawan, A. K., Rusdiana, D., Setiawan, W., Purnama, W., Fauzi, R.M., Fauzi, S. A., A. H.F. Alfani, A. H. F., and Arfiyogo, M. R. (2021). Design-construction of a solar cell energy water pump as a clean water source for people in Sirnajaya Village, Gununghalu district. *ASEAN Journal of Science and Engineering Education, 1*(1)*,* 15-20.

Irawan, A., Kurniawan, T., Alwan, H., Darisman, D., Pujianti, D., Bindar, Y., Bakar, M.S.A. and Nandiyanto, A.B.D. (2021). Influence temperature and holding time of empty fruit bunch slow pyrolysis to phenolic in biocrude oil. *Automotive Experiences*, *4*(3), pp.150-160.

Kareem, K., Rasheed, M., Liaquat, A., Hassan, A.M.M., Javed, M.I. and Asif, M. (2022). Clean energy production from jatropha plant as renewable energy source of biodiesel. *ASEAN Journal of Science and Engineering*, *2*(2), 193-198.

Kivevele, T., Raja, T., Pirouzfar, V., Waluyo, B., and Setiyo, M. (2020). LPG-fueled vehicles: An overview of technology and market trend. *Automotive Experiences, 3*(1), 6–19.

Lassen, T. (2013). Risk based fatigue inspection planning – state of the art. *Procedia Engineering, 66*(1877), 489–499.

Li, X., Koseki, H., and Mannan, M. S. (2015). Case study: Assessment on large scale LPG BLEVEs in the 2011 Tohoku earthquakes. *Journal of Loss Prevention in the Process Industries, 35*, 257–266.

Li, Y. Z. (2019). Study of fire and explosion hazards of alternative fuel vehicles in tunnels. *Fire Safety Journal, 110*, 102871.

DOI: http://doi.org/10.17509/ijost.v7i1.42916
p- ISSN 2528-1410 e- ISSN 2527-8045

Munahar, S., Purnomo, B. C., and Köten, H. (2021). Fuel control systems for planetary transmission vehicles: A contribution to the lpg-fueled vehicles community. *Mechanical Engineering for Society and Industry, 1*(1), 14–21.

Mzad, H., and Khelif, R. (2017). Numerical approach for reliability-based inspection periods (RBIP) of fluid pipes. *Case Studies in Thermal Engineering, 10*, 207-215.

Perumal, K. E. (2014). Corrosion risk analysis, risk based inspection and a case study concerning a condensate pipeline. *Procedia Engineering, 86*, 597–605.

Purnomo, B. C., and Widodo, N. (2019). Torque and power characteristics of single piston lpg-fueled engines on variations of ignition timing. *Automotive Experiences, 2*(1), 22-27.

Putri, B. M., Ningrum, L., Maulida, N. M. (2021). Simple micro-hydro uses water as a renewable energy source. *Indonesian Journal of Multidiciplinary Research, 1*(1), 23-28.

Rachman, A., and Ratnayake, R. M. C. (2019). Machine learning approach for risk-based inspection screening assessment. *Reliability Engineering and System Safety, 185*, 518–532.

Setiyo, M., Widodo, N., Purnomo, B. C., Munahar, S., Rahmawan, M. A., & Luthfi, A. Harvesting cooling effect on LPG-fueled vehicles for mini cooler: A lab-scale investigation. *Indonesian Journal of Science and Technology*, *4*(1), 39-47.

Shishesaz, M. R., Bajestani, M. N., Hashemi, S. J., and Shekari, E. (2013). Comparison of API 510 pressure vessels inspection planning with API 581 risk-based inspection planning approaches. *International Journal of Pressure Vessels and Piping, 111*, 202-208.

Sihombing, D. A., Yulianti, L., Prima E. C. (2021). Aloe vera as an alternative energy source. *Indonesian Journal of Multidiciplinary Research, 1*(1), 29-34.

Singh, M., and Pokhrel, M. (2018). A fuzzy logic-possibilistic methodology for risk-based inspection (RBI) planning of oil and gas piping subjected to microbiologically influenced corrosion (MIC). *International Journal of Pressure Vessels and Piping, 159*, 45-54.

Song, J. S., Lok, V., Yoon, K. B., Ma, Y. W., and Kong, B. O. (2021). Quantitative risk-based inspection approach for high-energy piping using a probability distribution function and modification factor. *International Journal of Pressure Vessels and Piping, 189*, 104281.

Susanto, R. M., Nurrochman, T., Munahar, S., and Ramadhan, A. I. (2019). Design and application of electronic tracking control systems (ETCS) to improve vehicle safety. *Automotive Experiences, 2*(3), 67–72.

Wang, G., Yan, T., Zhang, J., and Chen, J. (2011). Risk based Inspection on the equipment of low-density polyethylene. *Procedia Engineering, 15*, 1145–1148.

Widodo, E. M., Rosyidi, M. I., Purnomo, T. A., and Setiyo, M. (2019). Converting vehicle to LPG/Vigas: A simple calculator to assess project feasibility. *Automotive Experiences, 2*(2), 34–40.

DOI: http://doi.org/10.17509/ijost.v7i1.42916
p- ISSN 2528-1410 e- ISSN 2527-8045

Yi, H., Feng, Y., and Wang, Q. (2019). Computational fluid dynamics (CFD) study of heat radiation from large liquefied petroleum gas (LPG) pool fires. *Journal of Loss Prevention in the Process Industries, 61*, 262–274.

Zhang, Q., Qian, X., Fu, L., Yuan, M., and Chen, Y. (2020). Shock wave evolution and overpressure hazards in partly premixed gas deflagration of DME/LPG blended multi-clean fuel. *Fuel, 268*, 117368.

Zwetsloot, G., van Kampen, J., Steijn, W., and Post, S. (2020). Ranking of process safety cultures for risk-based inspections using indicative safety culture assessments. *Journal of Loss Prevention in the Process Industries, 64*, 104065.

DOI: http://doi.org/10.17509/ijost.v7i1.42916
p- ISSN 2528-1410 e- ISSN 2527-8045